Elsevier Editorial System(tm) for Ceramics International

Manuscript Draft

Manuscript Number:

Title: Graphene Derived Lanthanum Carbide targets for the SPES ISOL Facility

Article Type: Full length article

Keywords: Carbothermal reaction, multilayered graphene, sintering, carbides

Corresponding Author: Dr. Lisa Biasetto, Ph.D.

Corresponding Author's Institution: University of Padova

First Author: Stefano Corradetti

Order of Authors: Stefano Corradetti; Saramaria Carturan; Alberto Andrighetto; Gino Mariotto; Marco Giarola; Alberto Fabrizi; Lisa Biasetto, Ph.D.

Abstract: Lanthanum carbide based targets were produced as benchmark tests before the production of radioactive uranium carbide targets. Carbides possessing excess carbon and porosity seem to be the best candidates as target for the production of exotic beams in the SPES-ISOL facility. In addition, the capability of tailoring properties such as grains size and pores size represents a step ahead to improve the ions release efficiency.
In this work, multilayered graphene was used as source of carbon for the production of LaCx and the main physical properties of the produced targets were compared to standard LaCx produced using micrometric graphite. The main output of the work consisted in the reduced total porosity (28.8 vol% vs 47.8 vol%) and increased shrinkage (20.4 vol.% vs 5.8 vol.%) of the LaCx-Graphene samples compared to LaCx-Graphite ones. This result showed how graphene can be successfully employed as sintering aid for the sintering of carbides. Further studies are ongoing with UO2 as starting reagent for carburization within the project AUL-2013-16-176 "Study of the use of graphene as source of carbon for Uranium Carbide-Graphene nanocomposites production" now under conclusion at the JRC-ITU Actinide User Laboratory.

Suggested Reviewers: Gadipelli Srinivas
University College London
g.srinivas@ucl.ac.uk

Peter Kunz
TRIUMF
pkunz@triumf.ca

Toshihiro Isobe
Tokyo Institute of Technology
tisobe@ceram.titech.ac.jp

Opposed Reviewers:

Vicenza, April 11th 2017

COVER LETTER

Dear Editor,

on behalf of the all authors, I am sending to your attention the manuscript titled “Graphene Derived Lanthanum Carbide targets for the SPES ISOL Facility”. This research is the preliminary part of the project AUL-2013-16-176 “Study of the use of graphene as source of carbon for Uranium Carbide-Graphene nanocomposites production” now under conclusion at the JRC-ITU Actinide User Laboratory. This part of the research was run at INFN-LNL, University of Padova and University of Verona (Italy).

To the best of our knowledge, this is an original research work that studies the effect of graphene as carbon source for the production of carbides by carbothermal reaction. Our research show how the use of graphene as carbon source increases the densification of the newly formed carbides. We think that this research could be useful not only for the production of ISOL facilities targets, but in general for the sintering of covalent carbides.

Best Regards
Lisa Biasetto

1. Title: Graphene Derived Lanthanum Carbide targets for the SPES ISOL Facility

2. Authors: S. Corradetti[1], S.M. Carturan[1,2], A. Andrighetto[1], G. Mariotto[3], M. Giarola[3], A. Fabrizi[4], A. Maddalena[5] and L. Biasetto[1,4*]

3. Authors' affiliations:

[1] INFN-Laboratori Nazionali di Legnaro, Viale dell'Università 2, 35020 Legnaro (PD), Italy

[2] Università di Padova, Dipartimento di Fisica e Astronomia, Via Marzolo 8, I-35131 Padova, Italy.

[3] Università di Verona, Dipartimento di Informatica, Strada le Grazie 15, 37134, Verona, Italy

[4] Università di Padova, Dipartimento di Tecnica e Gestione dei Sistemi Industriali, Stradella San Nicola 3, 36100 Vicenza, Italy

[5] Università di Padova, Dipartimento di Ingegneria Industriale, Via Marzolo 9, 35131 Padova, Italy.

* Corresponding author at: Università di Padova, Dipartimento di Tecnica e Gestione dei Sistemi Industriali, Stradella San Nicola 3, 36100 Vicenza, Italy.

Tel: (+39) 044 499.8747;

E-mail: lisa.biasetto@unipd.it

4. Keywords
Carbothermal reaction, multilayered graphene, sintering, carbides

5. Highlights

1) Multilayered graphene was used for the very first time as carbon source for the carburization reaction of La_2O_3

2) The reaction kinetic showed a similar trend to the carburization of La_2O_3 using micrometric graphite.

3) The graphene derived LaC_x showed an impressively lower porosity (40 vol.% less) and higher shrinkage (70 vol.% more) than the graphite derived LaC_x samples.

4) From the results of the present work it is expected that graphene could be used as sintering aid for the production of fully dense carbides.

6. Abstract

Lanthanum carbide based targets were produced as benchmark tests before the production of radioactive uranium carbide targets. Carbides possessing excess carbon and porosity seem to be the best candidates as target for the production of exotic beams in the SPES-ISOL facility. In addition, the capability of tailoring properties such as grains size and pores size represents a step ahead to improve the ions release efficiency.

In this work, multilayered graphene was used as source of carbon for the production of LaC_x and the main physical properties of the produced targets were compared to standard LaC_x produced using micrometric graphite. The main output of the work consisted in the reduced total porosity (28.8 vol% vs 47.8 vol%) and increased shrinkage (20.4 vol.% vs 5.8 vol.%) of the LaC_x-Graphene samples compared to LaC_x-Graphite ones. This result showed how graphene can be successfully employed as sintering aid for the sintering of carbides. Further studies are ongoing with UO_2 as starting reagent for carburization within the project AUL-2013-16-176 "Study of the use of graphene as source of carbon for Uranium Carbide-Graphene nanocomposites production" now under conclusion at the JRC-ITU Actinide User Laboratory.

7. Introduction

The development of carbides possessing tailored functional properties is a topic of increasing interest for the production of targets for Isotope Separation On-Line (ISOL) Facilities [1, 2, 3, 4]. Within the target unit, high temperature (T=2000°C) and high vacuum ($p=10^{-4}$ Pa) are necessary to extract selected beams with high efficiency, though they drive the employed material to critical environmental conditions. For this reason, carbide based targets such as LaC_x, ThC_x, UC_x, SiC, TiC seem to be the best candidates for the production of neutron-rich and neutron deficient isotopes. The selected carbides can be synthesized via the classical carbothermal reaction, starting directly from oxides or from oxide generating precursors, such as acetates or oxalates [5], and a carbon source. In some cases (UC_x, LaC_x, ThC_x) the carbon in excess has the main role of dissipating the heat generated by the nuclear fission reactions occurring between the fissile atoms and the accelerated impinging beam, improving the high-temperature stability of the structure [6]. In addition, the presence of porosity and the grain size of carbides can affect respectively effusion and diffusion of the produced isotopes and consequently the release efficiency of the target [2]. For this reason, in the last few years, active research was run in order to understand the role of grain size and porosity on release efficiency properties of the target [2, 4]. The main output was the proved effect in terms of release efficiency and release times of nanostructured targets. The grain size affects the diffusion release, since diffusion constant is inversely proportional to grain size, while porosity and its interconnectivity degree affects the effusion. However, it should be noted that nanostructured targets must maintain their

nanostructures at the target operating temperature; for this reason grains growth and pores collapse must be avoided by mean of a proper design of the target material [7].

Within the SPES Project [8], much effort has been given to the development of carbides characterized by a tailored morphology as related to grains size and porosity. Lanthanum carbide was used as preliminary material for benchmark tests thereby avoiding the risks related to radioactivity.

Different carbon sources were used (graphite and MWCNTs) [9] as well as different lanthanum precursors (La_2O_3 and $La_2(C_2O_4)_3$) [5]. In addition, highly porous and interconnected cellular lanthanum carbide was developed [10, 11]. The same route was run using different uranium oxides sources (UO_2, U_3O_8 and UO_3) and carbon sources (graphite and MWCNTs) [1, 12]

The results of release efficiency of UC_x targets prepared starting from graphite and MWCNTs were recently reported in [13]. These materials proved to be interesting alternatives to the standard ones used in ISOL facilities [6, 14], where graphite is used as a carbon source; by means of the optimization of the production technique mechanically stable and high porosity samples were obtained.

Higher than ever yields of radioactive beams of selected isotopes have been indeed obtained using nanostructured targets, such as CaO or uranium carbide containing MWCNTs [4, 6].

Among the different allotropic configurations of carbon, graphene represents the most promising material, due to its unique physical, chemical and mechanical properties.

Graphene can be derived from thermal or chemical reduction process of graphene oxide (GO) and is called Reduced Graphene Oxide (RGO) or it can be obtained by mechanical exfoliation of graphite [15].

Because of its high accessible surface area and good electrochemical stability, graphene is widely used as active material or conductive substrate in energy storage devices [16, 17, 18]. Graphene and carbides can be find together in the literature for the synthesis of nanocomposites materials where graphene is used as reinforcing phase in carbide matrix composites [19, 20, 21]. Furthermore, graphene nanosheets play a key role on the sintering process (inhibiting the grain growth), so as on the mechanical properties of the material (increasing the material's toughness). To the best of our knowledge, only one experiment is reported in the literature where graphene is used as source of carbon for the synthesis of SiC nanoflakes [22].

One of the most common route to produce carbides is the carbothermal reduction process where the metal oxide is made to react with a source of carbon following reaction (1):

$$M_xO_y + (z+y+n)C \Rightarrow M_xC_z + yCO + nC \qquad (1)$$

This is a solid state reaction that occurs through solid state diffusion of carbon within the metal oxide lattice. The reaction occurs at high temperatures (T>1000°C) and takes long time to complete (several hours). In addition, the temperature must be further increased after carbothermal reaction is completed, in order to sinter the freshly formed carbide.

In [9], where MWCNTs were used as source of carbon, it was observed that the carbothermal reduction occurred at lower temperature than LaC_x obtained using graphite.

In the present work, commercial graphene was used as source of carbon for LaC_2 formation by means of carbothermal reaction run under high vacuum. The prepared samples were compared as for composition, structure and morphology to standard graphite-derived LaC_x samples in order to verify the reactivity of graphene with La_2O_3, thereby evaluating the possibility to exploit the well-known outstanding physical properties of graphene to enhance the final performances of the so obtained LaC_x composites.

This work is the preliminary step of the project titled AUL-2013-16-176 "Study of the use of graphene as source of carbon for Uranium Carbide-Graphene nanocomposites production" now under conclusion at the JRC-ITU Actinide User Laboratory.

8. Experimental

8.1 LaC_x synthesis

Lanthanum dicarbide–carbon composites were synthesized by means of the carbothermal reduction of lanthanum oxide, in the presence of excess carbon, according to reaction (1) reported above. Both graphite and graphene were used as carbon source, where the excess of carbon was calculated in order to obtain a final material with a LaC_2/C molar ratio equal to 1/2. La_2O_3 and graphite (mesh size <325 um) powders were purchased from Sigma–Aldrich and used as received. Elicarb® Graphene was purchased from Thomas Swan&Co. Ltd UK and used as received. The Elicarb® Graphene powders are high purity platelets of size ranging from 0.5 nm to 3 nm. Powders were manually mixed and grinded in an agate mortar where a 2–4 wt% of phenolic resin in acetone solution at 10 wt% was added as binder. Powders were uniaxially pressed at 750 MPa and after extraction were heat treated under high vacuum (10^{-3} Pa) in a graphite furnace [23], up to 1950 °C with a heating rate of 1 °C/min, no dwell time and a cooling rate of 5 °C/min.

Two kinds of samples were prepared, LaC_x-Graphite were prepared using graphite as source of carbon, whilst LaC_x-Graphene were prepared using graphene (details on the production and final properties are reported in Table 2).

Disks of 13 mm diameter and 1 mm thickness were prepared in a number of at least three samples for each composition.

8.2. Characterization

The composition of both the sintered samples and carbon sources were characterized by XRD (Bruker D8 Advance diffractometer, Karlsruhe, Germany), using CuKα radiation$\lambda\lambda$= 1.5412 Å, at 40 kV and 40 mA. The 2ϑ range was varied from 25° to 80° with a step size of 0.05° and a step time of 5 s. The quantitative analyses of the phases present after sintering so as the crystallite size were calculated by Rietveld method using MAUD [24]. The crystalline phases structure was identified by Crystalline Open

Database (COD) [25]. The microstructure of the LaC_x samples was characterized by a scanning electron microscope (SEM Vega 3xmh, Tescan, Brno, Czech Republic), equipped with an energy-dispersive X-ray spectroscopy (EDS-EDAX) detector.

The graphene and graphite powders were also observed by Transmission Electron Microscopy (TEM). The micrographs of the as received carbon materials were acquired by means of a JEOL JEM 2000 EX-II microscope operating at 200 keV. TEM samples were prepared by dispersing the carbon powders in ethanol; then, a drop of the suspensions was deposited on a 200-mesh copper TEM grid coated with a thin amorphous carbon film.

Raman spectroscopy was used to characterize both the as received carbon powders (both graphene and pyrolytic graphite) and the graphene and graphite derived LaC_x samples. Micro-Raman spectra were carried out in backscattering geometry using a Horiba-Jobin Yvon apparatus, model LabRam HR, consisting of a single spectrograph, with a focal length of 80 cm, and mounting a holographic grating (600 lines/mm), to disperse the anelastically scattered radiation. The system exploited a narrow band notch filter to reject the elastically scattered light. The spectra here reported were excited by the 633 nm line of a He-Ne laser through an objective 80X, and recorded by a CCD (256x1024 pixels) detector, cooled at -134 °C. The maximum laser power flux impinging the samples, without filters, can be estimated of the order of 10^9 W/m^2, critically depending on the focusing precision. In order to prevent sample overheating and possible related damage it can be reduced in a controlled manner to the optimal value by using neutral filters of optical density ranging from 0.3 up to 4.

The samples bulk density was measured as mass over volume ratio and the total porosity was calculated by eq.2:

$$P_{tot} = 1 - \frac{\rho_{bulk}}{\rho_{th}} \qquad \text{(eq.2)}$$

where the ρ_{bulk} is the bulk density and the ρ_{th} was calculated by the rule of mixture, taking into account the volumetric fractions of LaC_2 and free carbon present in the final samples (Eq.1) and their theoretical solid densities, 5.29 g/cm^3 for LaC_2 [26] and 1.90 g/cm^3 for graphite (as of producer datasheet). Analogously to previous studies performed with carbon nanotubes [5, 9], also in this case no information on the actual graphene density was obtainable, so the same value of graphite was initially used for porosity calculation purposes. However, since literature reports values for graphene densities that span from 1.9 to 2.3 g/cm^3, porosity calculations were performed in this work also considering the latter case, as reported in the next section.

The shrinkage of the samples was measured as volume variation before and after sintering.

The specific surface area (SSA) and the presence of micro-meso porosity were estimated by N_2 physisorption measurements (ASAP2020, Micromeritics, Norcross, GA), using the classical Brunauer-Emmett-Teller (BET) model to derive SSA values and the Barrett–Joyner–Halenda (BJH) method for pores size investigation.

9. Results and Discussion

In figure 1 the XRD analyses of both the a.r. graphite and graphene powders are reported. The XRD spectra measured in the range 10°-50° show (002) diffraction peak at 2θ=26.45° (a.r. Graphite) and 2θ=26.55° (a.r. Graphene), which is related to the distance between graphene layers [27]. The graphite spectrum also presents a peak splitting, resulting in the presence of a minor peak at 25.5°. Results are reported in Figure 1.

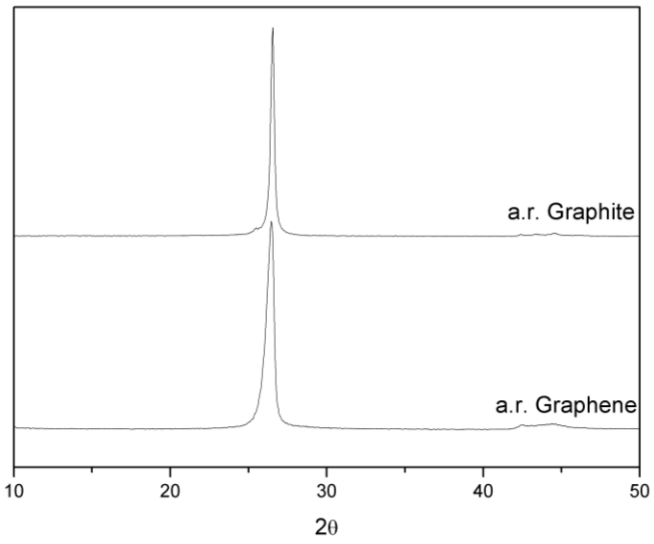

Figure 1 – Graphite and Graphene Diffraction patterns

In Raman spectra (Figure 2) the presence of the G' band, with multiple curves fitting, confirms the multilayered structure of the graphene used in this work [28]. Monolayer graphene usually displays a single, Lorentzian shaped peak in the G' position and its intensity is much higher than the G band, while multilayered structure in graphene leads to multi-component peak for G' band and strongly reduced intensity, with remarkable affinity with highly ordered pyrolytic graphite (HOPG) spectral features [29].

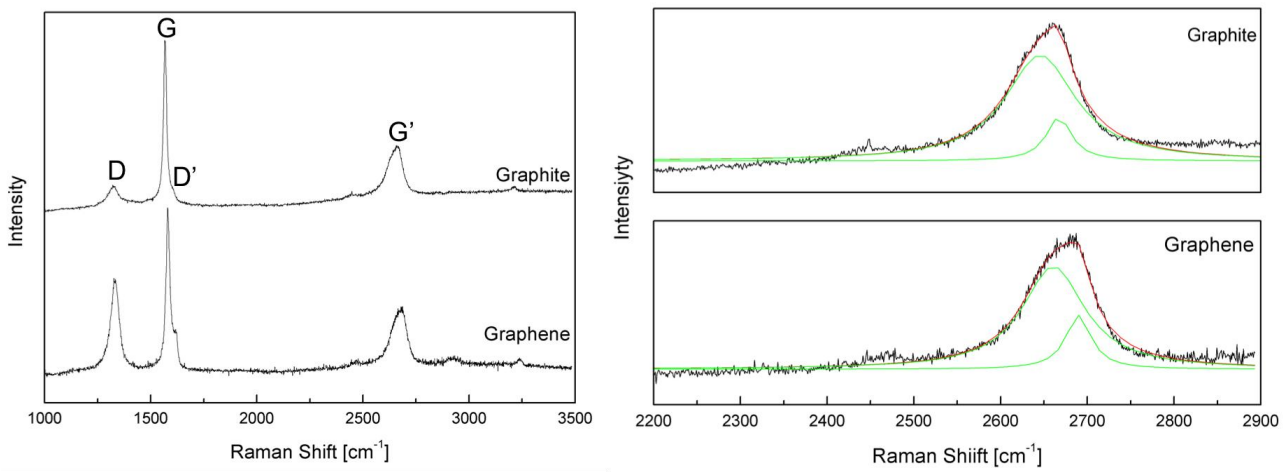

Figure 2- Left: Raman spectra of a.r. graphene and graphite; right: Lorentian peak fitting.

Table 1-Stacking layers calculation for a.r Graphene and Graphite

	I_D/I_G	L_a [nm]
Graphite	0.38	44.3
Graphene	1.08	15.6

The nanocrystallite size, L_a, can be derived from the ratio Id/Ig as detailed in [30]: for graphite the estimated L_a value is 44.3 nm, while for graphene is 15.6 nm (λexc 514.5 nm).

The intensity of the D band, generally associated to the presence of defects, increases in graphene as compared to graphite. This trend can be associated to the reduced grain size of graphene and consequently to the presence of defects associated to grain boundaries. As stated by Cançado and co-workers [31], the amount of disorder in a nanocrystallite is given by the extent of border (one-dimensional defects) with respect to the total crystallite area, that is L_a. Therefore, the increase of the D band intensity for the case of graphene used in this study can be associated to the increase of the ratio between grain boundaries width and grain size (L_a) (Table 1).

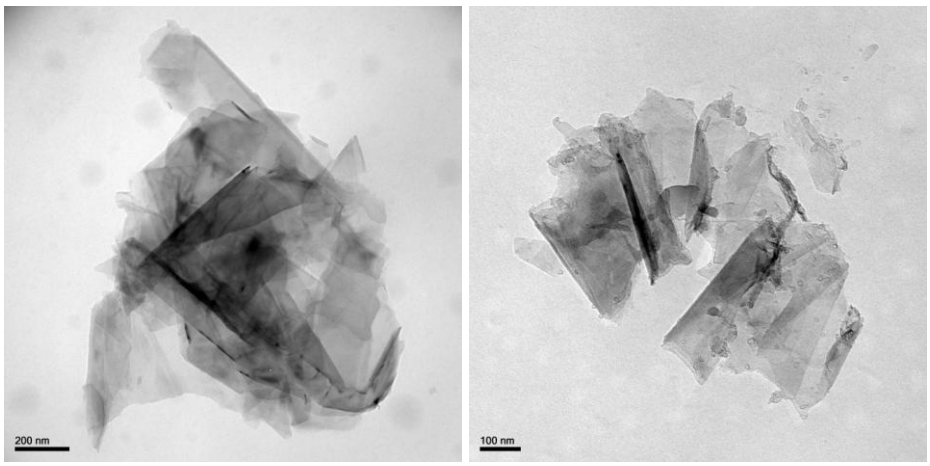

Figure 3- TEM micrographs of as received a) graphene and b) graphite powders.

Representative bright-field TEM images of the provided graphite and graphene powders are shown in Fig. 3 a and b, respectively. Both carbon materials clearly show an evident platelet-like morphology and the size of the sheets, often stacked one to each other, ranges from several microns to a few hundred nanometers.

An overview of the produced samples in terms of shrinkage, weight loss and calculated porosity is reported in Table 2. It can be observed the impressively higher shrinkage for LaC_x-Graphene sample (20.4±3.1 %) compared to LaC_x-Graphite (5.8±0.6%). This is associated to a reduction of total porosity

for LaC_x-Graphene (28.9±2.2% considering a graphene density of 1.9 g/cm^3 or 32.6±2.1% considering a graphene density of 2.3 g/cm^3) versus 47.8±1.0% of LaC_x-Graphite. On the other hand, the weight loss for the two type of samples is quite similar, with a slightly higher weight loss for LaC_x-Graphite, thus proving that the reaction proceeds in both cases at quite the same extent.

Table 2- Composition, shrinkage, weight losses and calculated total porosity of the produced samples. [a] Data for $\rho\rho_{graphene}$ = 1.9 g/cm^3, [b] data for $\rho\rho_{graphene}$ = 2.3 g/cm^3

	Composition			Density [g/cm^3]	Shrinkage [vol.%]	Weight loss [wt.%]	Theoretical weight loss [wt.%]	Total porosity [vol.%]
Sample	**La_2O_3 [wt.%]**	**Graphite [wt.%]**	**Graphene [wt.%]**					
LaCx-Graphite	71.2	28.8	-	3.1 ± 0.1	5.8 ± 0.6	23.8 ± 0.3	18.4	47.8 ± 1.0
LaCx-Graphene	71.2	-	28.8	2.2 ± 0.1	20.4 ± 3.1	22.2 ± 0.2	18.4	28.9 ± 2.2[a] 32.6 ± 2.1[b]

The base pressure versus temperature during the whole process in the vacuum chamber, as reported in Figure 4 for a batch of two LaC_x-Graphene and two LaC_x-Graphite samples treated simultaneously. The reported gas release is very similar to the ones already reported for LaC_x-Graphite [9], with the samples outgassing and the phenolic resin decomposition occurring in the 200-800 °C region and carbothermal reaction starting between 1100 °C and 1200 °C. Therefore, negligible differences in the reactivity of the starting mixtures either employing graphite or graphene can be inferred. As reported in a previous study [5], additional gas release occurred for temperatures above 1700 °C which could be attributable to both the furnace outgassing and the LaC_2 sublimation from the pellets surfaces. This latter phenomenon could also explain the higher weight loss of the treated samples with respect to the theoretical ones which were calculated basing on stoichiometry, as reported in Table 2 and discussed in [5].

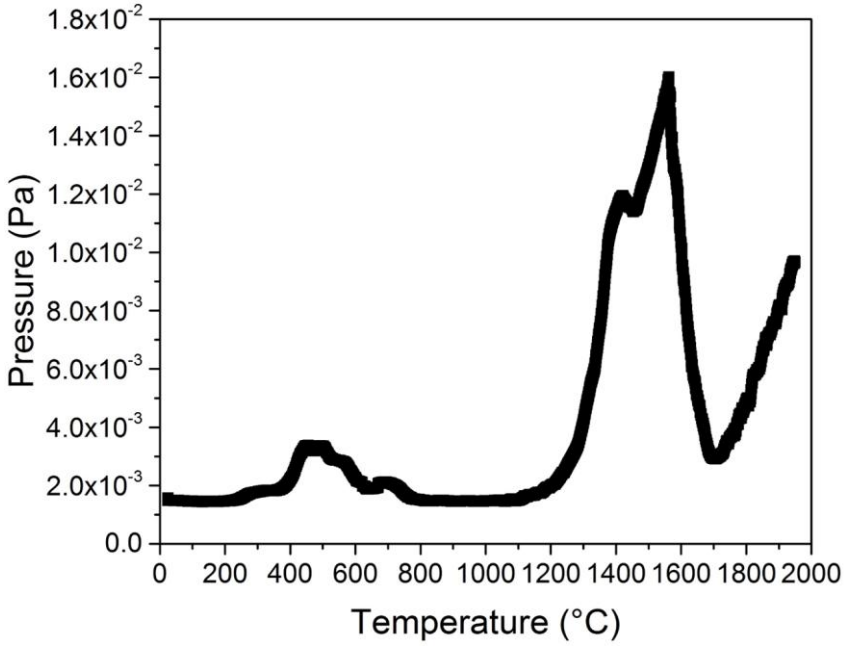

Figure 4- Gas evolution upon carburization and sintering of graphene and graphite derived LaC_x (two samples for each composition treated together).

Previous results with MWCNT as carbon source have shown higher reactivity as compared to graphite [9]: the carburization reaction starts at 1000 °C and is complete at 1400 °C, whereas for graphite-based composites the reaction starts at 1200 °C and is still ongoing at 1400 °C. In that case, the activation energy of the carbothermal reaction is clearly reduced by the presence of the nanotubes: the reaction proceeds either by direct contact between carbon and the oxide or by diffusion of carbon through the newly formed carbide grains and reaction with the oxide. Then, CO evolution occurs as a by-product of the reaction. The presence of MWCNT favours both the contact between reactants, owing to their high aspect ratio leading to more intimate contact with oxide powders, and the easier release of gaseous products, owing to the presence of nano-sized tubular channels. In the case of multi-layered graphene used herein, the observed similar reactivity as compared to graphite leads to the conclusion that agglomeration of multilayered graphene and phase separation between oxide and graphene itself occurs, thus leading to interfacial contact between the two phases quite similar to the case of graphite. The expected intercalation of oxide powders between the 2D-platelets does not take place and different techniques of mixing should be investigated to avoid agglomeration. On the other hand, the possibility that using a graphene with higher aspect ratio, composed of fewer layers of sp^2 carbon atoms, could sensibly modify the interfacial contact and increase the reactivity cannot be ruled out.

On the other hand, a quite impressive shrinkage in the case of graphene-derived composites is observed. The much higher densification degree can be ascribed to a sintering-aid effect induced by the graphene nanoplatelets. This behaviour has been previously reported in literature for the case of other carbides such as B_4C and TiC [19, 20, 21] and will be discussed below in more detail.

Differences in densities of LaC_x-Graphite with respect to previously reported data [5, 9] could be ascribed to differences in the thermal treatment. In past studies indeed the treatments were divided into many substeps including heating at 2 °C/min and extremely long dwell times (9, 12 or 24 hours), whereas in this case a continuous, although slower in terms of rate, heating was performed up to very high temperatures.

N_2 adsorption-desorption isotherms of samples obtained using either graphite or graphene are reported in Figure 5, with pores size distribution as derived by BJH method.

In the case of graphite derived samples the SSA is almost negligible and approaching the sensitivity of the technique, around 1 m^2/g, irrespectively of the heating rate during treatment and in agreement with previously reported data [9]. The isotherm recorded for purified graphene is reported in the inset graph of Figure 5. The estimated BET value for SSA is only 29 m^2/g, a surprisingly low value for graphene, taking into account that the powder has been treated with sonication in N-methyl pyrrolidone and filtered with a Teflon membrane (pore size 2.5 μm) prior to analysis in order to

separate possible stacked layers [32]. On the other hand, this result is in agreement with XRD and Raman analyses, which point to a tight packing of several graphene sheets, and with previously reported N_2 physisorption data on multi-layered graphene [33].

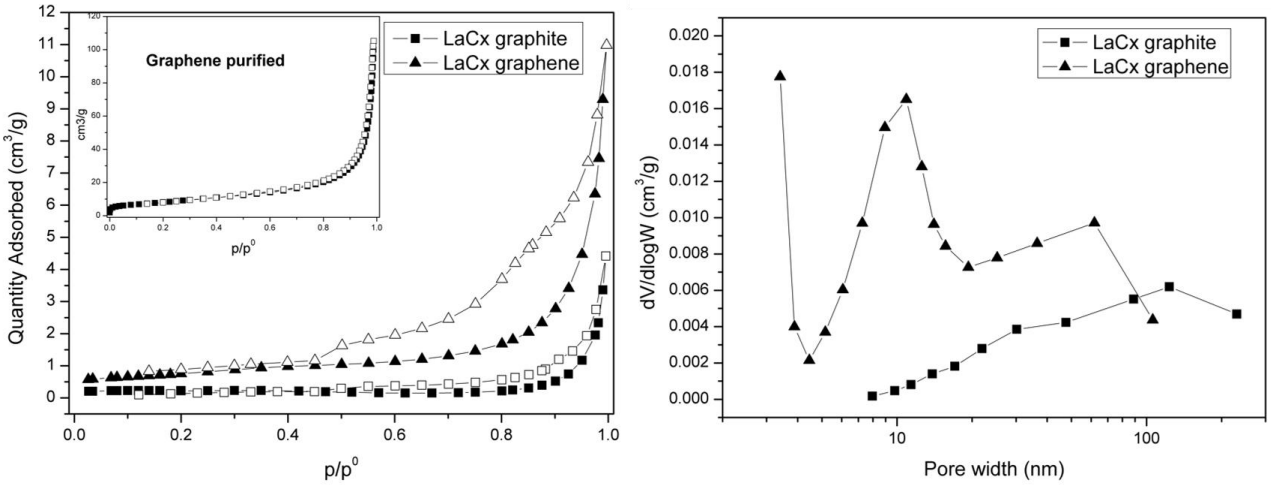

Figure 5- N_2 adsorption-desorption isotherms for LaCx composites derived from graphite or graphene (left side, inset graph graphene after purification) and pore size distribution as derived from BJH model (right side).

Since the interlayer distance of graphene is around 0.34 nm, from XRD estimation, most of the packed layers are inaccessible by liquid nitrogen molecule, thus resulting in dramatically reduced SSA with respect to the theoretical SSA for graphene single layers (2620 m^2/g) [34]. For samples obtained from graphene as carbon source, a very weak increase in SSA can be noticed and values around 2.8 m^2/g are estimated using the BET algorithm. The isotherm is of type IV according to IUPAC classification [35], the hysteresis loop extends up to the high pressure regime indicating the presence of mesopores of large size (around 10 nm), as confirmed by BJH analysis performed on the desorption branch.

XRD investigations, reported in Figure 6, show the formation of only $\alpha -LaC_2$ for both samples, as confirmed by the good Rietveld fitting.

It is worth to note that the presence of residual carbon cannot be detected by the XRD analyses due to the presence of the high atomic number lanthanum atoms. The Rietveld analyses show that LaC_x-Graphite samples possess an asymmetric shape with crystallites of about 32 nm size in the [112] direction, whilst on [110] direction a size of about 85 nm. As concern the LaC_2 crystallites in LaC_x-Graphene samples, they also possess an asymmetric shape, thus giving in the [112] direction a size of about 27 nm, whilst on [110] direction a size of about 55 nm.

The small inserts in figure 7a and c, where SEM images of the samples surface are reported, show the aspect of the composites after thermal treatment: the LaC_x- Graphite sample shows a dark-grey color with small bright spots, the LaC_x-Graphene sample shows a light yellow colour with some grey spots. This difference can be attributed both to the higher amount of porosity in LaC_x-Graphite and to the less efficient dispersion of carbon among the LaC_x grains. This is confirmed by the SEM images reported in

Figure 7 where the higher level of dispersion of carbon in LaC_x-Graphene sample is clearly observed. The high magnification images in Figure 7b and d and their inserts show the formation of micron-sized grains, as detected on the sample surface. The observation at high magnification of the samples cross-section, as shown in Figure 8, clearly evidences the enhanced degree of compaction in graphene-derived composite.

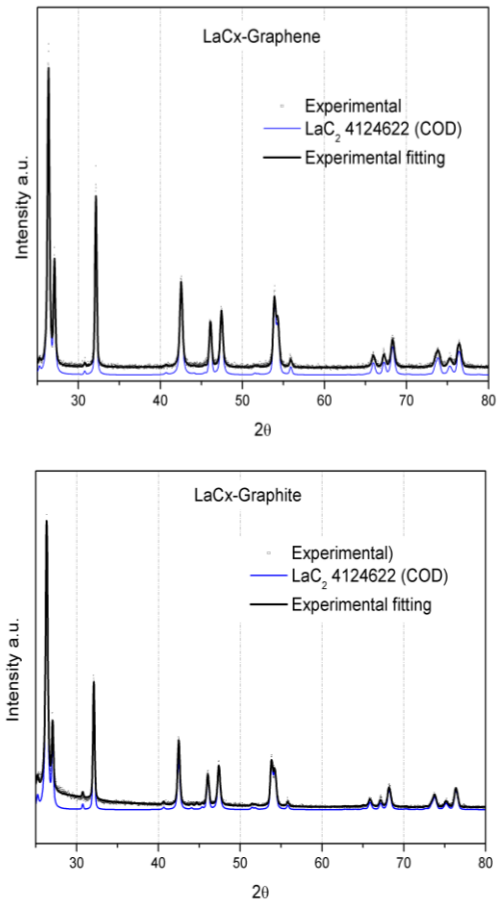

Figure 6- Top, XRD diffraction of LaC_x-Graphene; bottom XRD pattern of LaC_x-Graphite

The data on porosity and SEM images point to a possible scenario where enhanced densification occurs in the samples in the case of residual graphene after the carbothermal reaction. In fact, the carburization process displays almost the same features as for starting temperature, CO evolution with temperature and time and final yield, either using graphene or graphite as starting reactant. As soon as carburization reaches the maximum extent, the role of residual multilayered graphene changes to that of a sintering-aid, hence smaller grains, higher compaction and little or no porosities develop in this system as compared to graphite-based one.

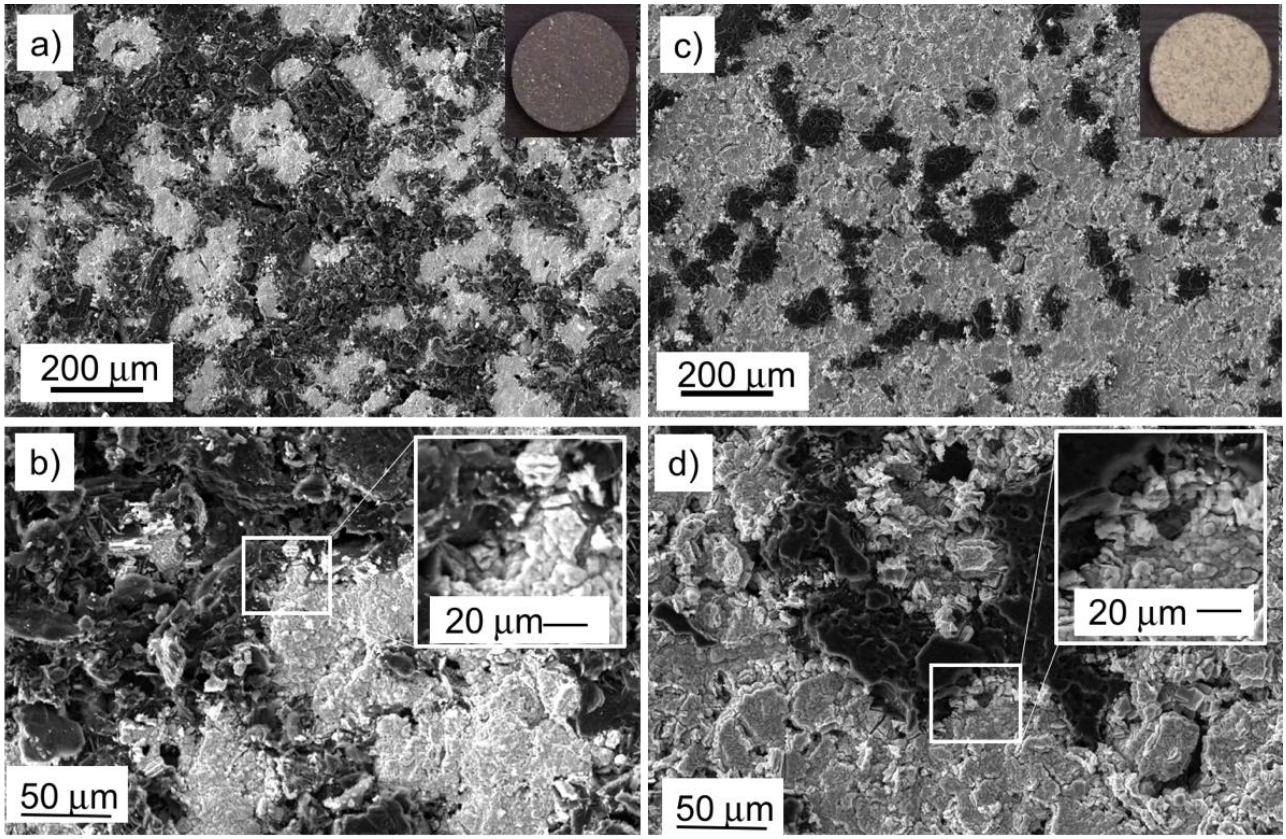

Figure 7-SEM images of LaC_x-Graphite (a,b) and LaC_x-Graphene(c,d). The inserts in figures a and c show the samples after thermal treatment.

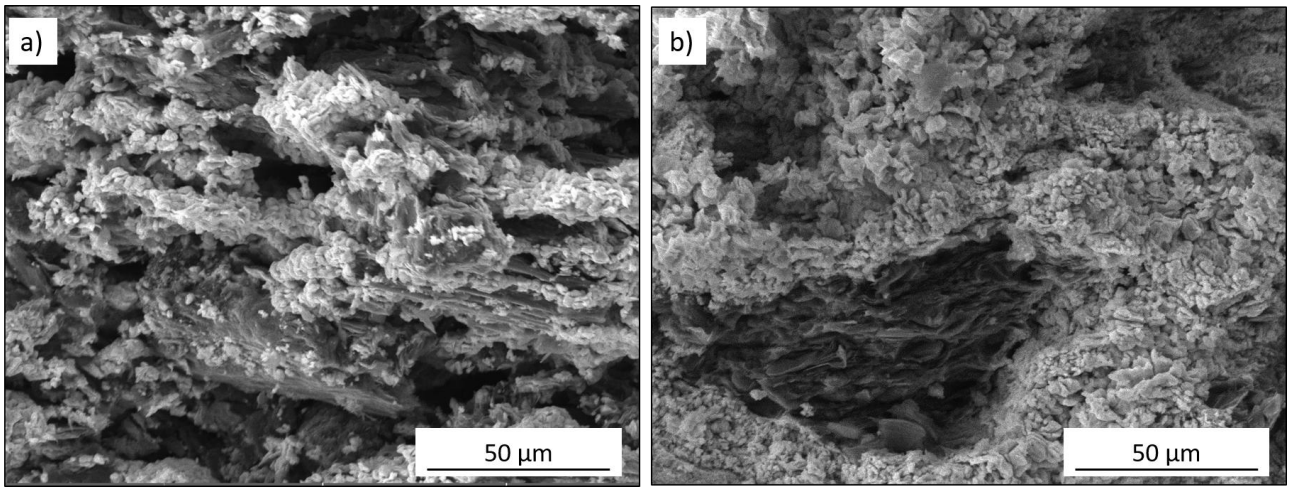

Figure 8. SEM images of the cross-section of the samples derived from graphite (a) and graphene (b) taken at the same magnification (1600x).

Micro-Raman spectra of the sintered carbides are shown in Figure 9. The spectra recorded from unreacted grains of either graphite or graphene derived samples clearly show the typical fingerprints of crystalline sp2 carbon. i.e.: D, G and G' bands (Fig. 9, top panel). The spectra collected from the bright grains of both graphite and graphene derived samples, do not show any Raman mode of the

LaC_x phase, but only the D and G bands of the residual carbon (Fig. 9, bottom panel). In fact, the G' band at high wavenumbers is no longer observed. Moreover, the ratio I_D/I_G is much higher in these spectra as compared to the spectra from dark grains, coming from unreacted, massive carbon, either graphite or graphene. All these features strongly point to a remarkable amorphization of the carbonaceous residual phase. A further evidence of this structure modification is the reduced intensity of the D band in the unreacted graphene, as compared to the as received graphene (see, Fig. 2, left panel). Since sintering is a diffusion driven process, it can be expected that the higher amount of defects present in the multilayered graphene used in this work become active during sintering, thus reducing the gradient of defects concentration between graphene grain boundaries.

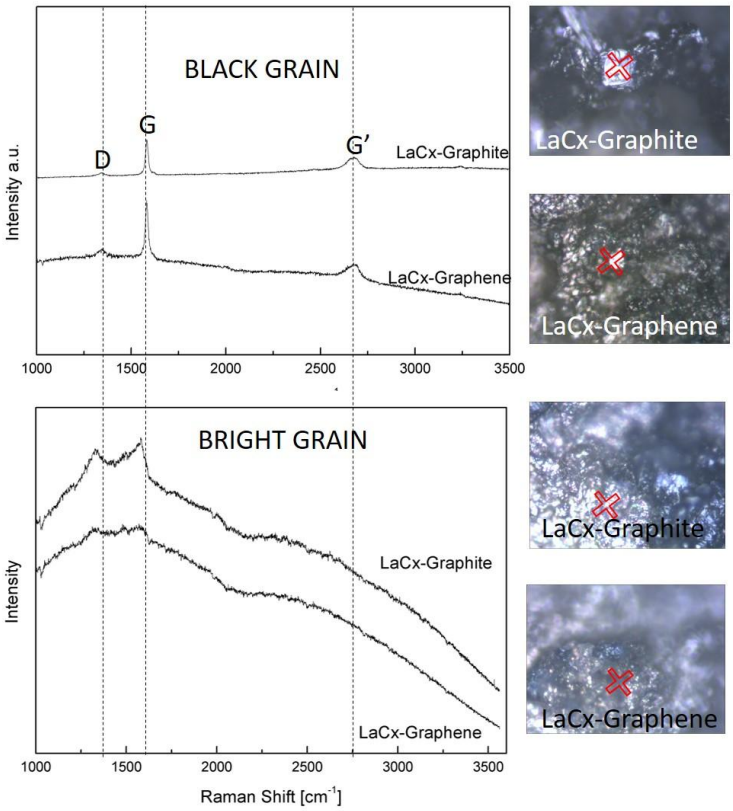

Figure 9- Raman spectra of LaC_x-Graphite and LaC_x-Graphene samples (black grain, unreacted carbon, while bright grain is the LaC_x grain.

10. Conclusions

Multilayered graphene as source of carbon for the carbothermal reaction of La_2O_3 has been chosen in this study and this approach has been compared with the traditional use of standard graphite. Main results revealed that multilayered graphene does not act as a catalyst for the carburization reaction, as was expected from previously observed behavior of MWCNTs as carbon source. The negligible effect of the presence of multilayer graphene on the thermodynamics of the whole process can be ascribed to the fact that the graphene used in this work is mainly composed of agglomerated and the reactivity is similar to graphite due to the comparable SSA between the two reactants.

However, it should be observed how the use of graphene leads to the production of composites with remarkably enhanced reduction of porosity of the 40 vol.% if compared to LaC_x-Graphite samples, meanwhile displaying an increase of the shrinkage of the 70 vol.%. These data drive to the conclusion that the multilayered graphene used in this work can be effectively used as sintering aid for lanthanum carbides production, and that this effect could be extendable to other carbides. The role of graphene as sintering aid is still under study, however the experiments herein described give evidence that it becomes active at temperatures higher than 1250°C, that is the temperature at which the carbothermal reaction starts to occur.

11. References

[1] L. Biasetto, P. Zanonato, S. Carturan, P. Di Bernardo, P. Colombo, A. Andrighetto, G. Prete, Developing uranium dicarbide–graphite porous materials for the SPES project, J. Nucl. Mater. 404 (2010) 68-76.

[2] B. Hy, N. Barré-Boscher, A. Ozgumus, B. Roussiere, S. Tusseau-Nenez, C. Lau, M. Cheikh Mhamed, M. Raynaud, A. Said, K. Kolos, E. Cottereau, S. Essabaa, O. Tougait, M. Pasturel, An off-line method to characterize the fission product release from uranium carbide-target prototypes developed for SPIRAL2 project, Nucl. Instrum. Methods Phys. Res. B 288 (2012) 34-41.

[3] T. Storà, Recent developments of target and ion sources to produce ISOL beams, Nucl. Instrum. Methods Phys. Res. B 307 (2013) 402-410.

[4] J.P. Ramos, A. Gottberg, R.S. Augusto, T.M. Mendonca, K. Riisager, C. Seiffert, P. Bowen, A.M.R. Senos, T. Stora, Target nanomaterials at CERN-ISOLDE: synthesis and release data, Nucl. Instrum. Methods Phys. Res. B 376 (2016) 81–85.

[5] L. Biasetto, P. Zanonato, S. Carturan, P. Di Bernardo, P. Colombo, A. Andrighetto, G. Prete, Lanthanum carbide-based porous materials from carburization of lanthanum oxide and lanthanum oxalate mixtures, J. Nucl. Mater. 378 (2008) 180-187.

[6] A. Gottberg, Target materials for exotic ISOL beams, Nucl. Instrum. Methods Phys. Res. B 376 (2016) 8-15.

[7] J. Guillot, S. Tusseau-Nenez, B. Roussière, N. Barré-Boscher, F. Brisset, M. Cheikh Mhamed, C. Lau, S. Nowak, Study of uranium oxide milling in order to obtain nanostructured UC_x target, Nucl. Instrum. Methods Phys. Res. B 374 (2016) 116-120.

[8] A. Monetti, A. Andrighetto, C. Petrovich, M. Manzolaro, S. Corradetti, D. Scarpa, F. Rossetto, F. Martinez Dominguez, J. Vasquez, M. Rossignoli, M. Calderolla, R. Silingardi, A. Mozzi, F. Borgna, G. Vivian, E. Boratto, M. Ballan, G. Prete, G. Meneghetti, The RIB production target for the SPES project, Eur. Phys. J. A 51 (2015) 128-138.

[9] L. Biasetto, S. Carturan, G. Maggioni, P. Zanonato, P. Di Bernardo, P. Colombo, A. Andrighetto, G. Prete, Fabrication of mesoporous and high specific surface area lanthanum carbide–carbon nanotube

composites, J. Nucl. Mater. 385 (2009) 582-590.
[10] L. Biasetto, M.D.M. Innocentini, W.S. Chacon, S. Corradetti, S. Carturan, P. Colombo, A. Andrighetto, Gas permeability of lanthanum oxycarbide targets for the SPES project, J. Nucl. Mater. 440 (2013) 70-80.
[11] S. Corradetti, L. Biasetto, M.D.M. Innocentini, S. Carturan, P. Colombo, A. Andrighetto, Use of polymeric fibers to increase gas permeability of lanthanum carbide based targets for nuclear physics applications, Ceram. Int. 42 (2016) 17764-17772.
[12] S. Corradetti, L. Biasetto, M. Manzolaro, D. Scarpa, S. Carturan, A. Andrighetto, G. Prete, J. Vasquez, P. Zanonato, P. Colombo, C.U. Jost, D.W. Stracener, Neutron-rich isotope production using a uranium carbide–carbon nanotubes SPES target prototype, Eur. Phys. J. A 49 (2013) 56.
[13] S. Tusseau-Nenez, B. Roussière, N. Barré-Boscher, A. Gottberg, S. Corradetti, A. Andrighetto, M. Cheikh Mhamed, S. Essabaa, H. Franberg-Delahaye, J. Grinyer, L. Joanny, C. Lau, J. Le Lannic, M. Raynaud, A. Saïd, T. Stora, O. Tougait, Characterization of uranium carbide target materials to produce neutron-rich radioactive beams, Nucl. Instrum. Methods Phys. Res. B 370 (2016) 19-31.
[14] S. Corradetti, L. Biasetto, M. Manzolaro, D. Scarpa, A. Andrighetto, S. Carturan, G. Prete, P. Zanonato, D.W. Stracener, Temperature dependence of yields from multi-foil SPES target, Eur. Phys. J. A 47 (2011) 119.
[15] F. Bonaccorso, A. Lombardo, T. Hasan, Z. Sun, L. Colombo, A. C. Ferrari, Production and processing of graphene and 2d crystals, Mater. Today 15 (2012) 564-589.
[16] Y. Wang, Z. Shi, Y. Huang, Y. Ma, C. Wang, M. Chen, Y. Chen, Supercapacitor Devices Based on Graphene Materials, J. Phys. Chem. C 113 (2009) 13103–13107.
[17] B.G. Choi, M. Yang, W.H. Hong, J.W. Choi, Y.S. Huh, 3D Macroporous Graphene Frameworks for Supercapacitors with High Energy and Power Densities, ACS Nano 6 (2012) 4020–4028.
[18] D. Chen, L. Tang, J. Li, Graphene-based materials in electrochemistry, Chem. Soc. Rev. 39 (2010) 3157–3180.
[19] X. Liu, J. Li, X. Yu, H. Fan, Q. Wang, S. Yan, L. Wang, W. Jiang, Graphene nanosheet/titanium carbide composites of a fine-grained structure and improved mechanical properties, Ceram. Int. 42 (2016) 165–172.
[20] L. Liu, Y. Wang, X. Li, L. Xu, X. Cao, Y. Wang, Z. Wang, C. Meng, W. Zhu, X. Ouyang, Enhancing Toughness in Boron Carbide with Reduced Graphene Oxide, J. Am. Ceram. Soc. 99 (2016) 257–264.
[21] M. Chen, J. Zhang, Q. Chen, M. Qi, X. Xia, Construction of reduced graphene oxide supported molybdenum carbides composite electrode as high-performance anode materials for lithium ion batteries, Mater. Res. Bull. 73 (2016) 459–464.
[22] S. Chabi, H. Chang, Y. Xia, Y. Zhu, From graphene to silicon carbide: ultrathin silicon carbide flakes, Nanotechnology 27 (2016) 602-609

[23] S. Corradetti, A. Andrighetto, M. Manzolaro, D. Scarpa, J. Vasquez, M. Rossignoli, A. Monetti, M. Calderolla, G. Prete, Research and development on materials for the SPES target, Eur. Phys. J. Web Conf. 66 (2014) 11009.
[24] L. Lutterotti, Total pattern fitting for the combined size-strain-stress-texture determination in thin film diffraction, Nucl. Instrum. Methods Phys. Res. B 268 (2010) 334-340.
[25] S. Grazulis, D. Chateigner, R.T. Downs, A.T. Yokochi, M. Quiros, L. Lutterotti, E. Manakova, J. Butkus, P. Moeck, A. Le Bail, Crystallography Open Database – an open-access collection of crystal structures, J. Appl. Cryst. 42 (2009) 726-729.
[26] D.L. Perry, Handbook of Inorganic Compounds, second Edition, CRC Press, Boca Raton, FL, USA, 2011.
[27] L. Stobinski, B. Lesiak, A. Malolepszy, M. Mazurkiewicz, B. Mierzwa, J. Zemek, P. Jiricek, I. Bieloshapka, Graphene oxide and reduced graphene oxide studied by the XRD, TEM and electron spectroscopy methods, J. Electron Spectrosc. Relat. Phenom. 195 (2014) 145-154.
[28] Z. Ni, Y. Wang, T. Yu, Z. Shen, Raman Spectroscopy and Imaging of Graphene, Nano Res. 1 (2008) 273-291.
[29] A. Jorio, Raman Spectroscopy in Graphene-Based Systems: Prototypes for Nanoscience and Nanometrology, ISRN Nanotechnol. 2012 (2012) 234216.
[30] L.G. Cançado, K. Takai, T. Enoki, General equation for the determination of the crystallite size La of nanographite by Raman spectroscopy, Appl. Phys. Lett. 88 (2006) 163106.
[31] L.G. Cançado, A. Jorio, E.H. Martins Ferreira, F. Stavale, C.A. Achete, R.B. Capaz, M.V.O. Moutinho, A. Lombardo, T.S. Kulmala, A.C. Ferrari, Nano Lett. 11 (2011) 3190–3196.
[32] G. Srinivas, Y. Zhu, R. Piner, N. Skipper, M. Ellerby, R. Ruoff. Synthesis of graphene-like nanosheets and their hydrogen adsorption capacity, Carbon 48 (2009) 630-635.
[33] K.S. Subrahmanyam, S.R.C. Vivekchand, A. Govindaraj, C.N.R. Rao, A study of graphenes prepared by different methods: characterization, properties and solubilization, J. Mater. Chem. 18 (2008) 1517–1523.
[34] D.W. Wang, F. Li, Z.S. Wu, W.C. Ren, H.M. Cheng, Electrochemical interfacial capacitance in multilayer graphene sheets: Dependence on number of stacking layers et al., Electrochem. Commun. 11 (2009) 1729–1732.
[35] K.S.W.Sing, D.H.Everett, R.A.W.Haul, L.Moscou, R.A.Pierotti, J.Rouquerol, T.Siemieniewska, Reporting physisorption data for gas/solid systems with special reference to the determination of surface area and porosity, Pure Appl. Chem. 57 (1985) 603–619.

Figure 1

Click here to download high resolution image

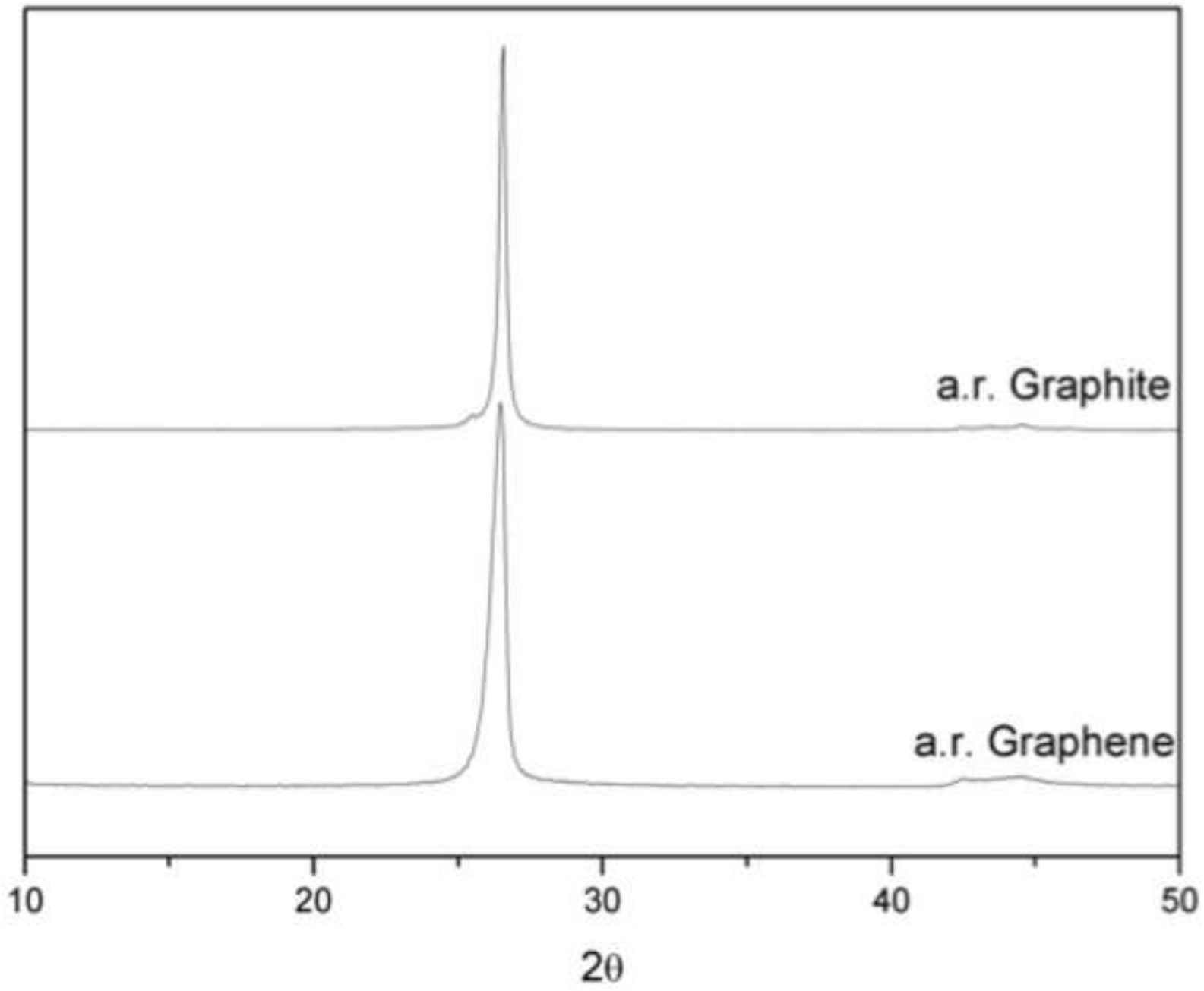

Figure 2

Click here to download high resolution image

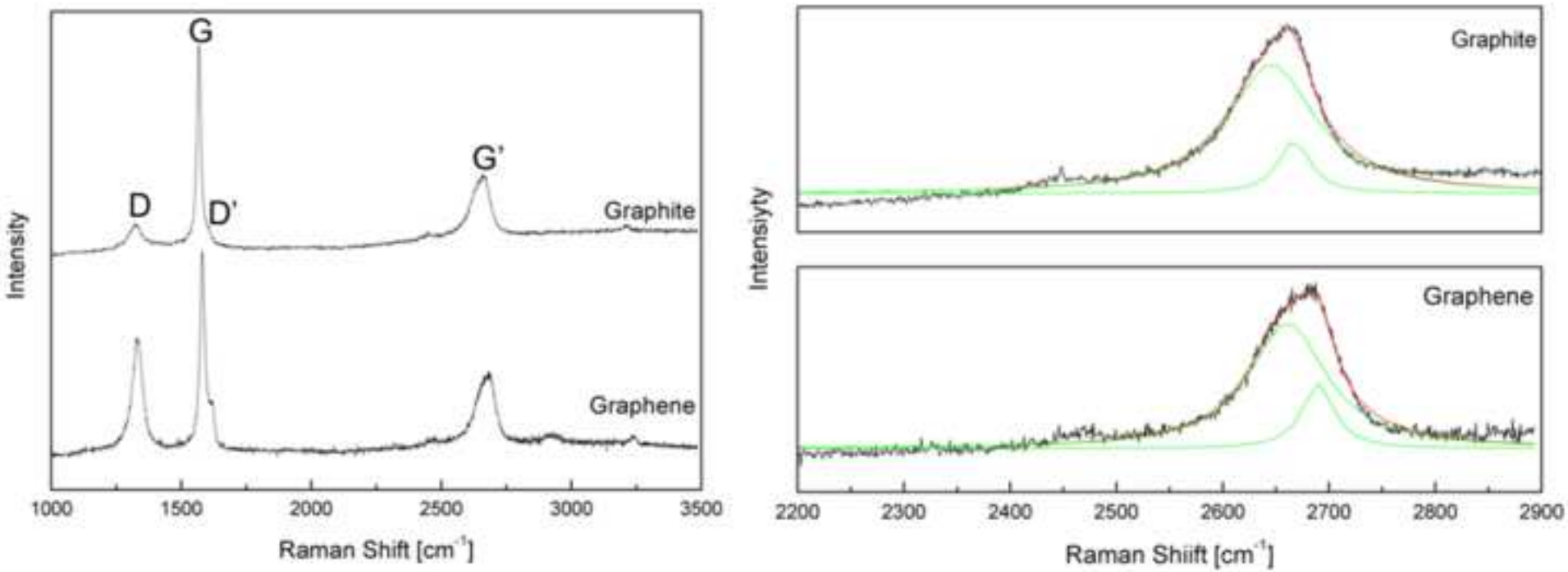

Figure 3

Click here to download high resolution image

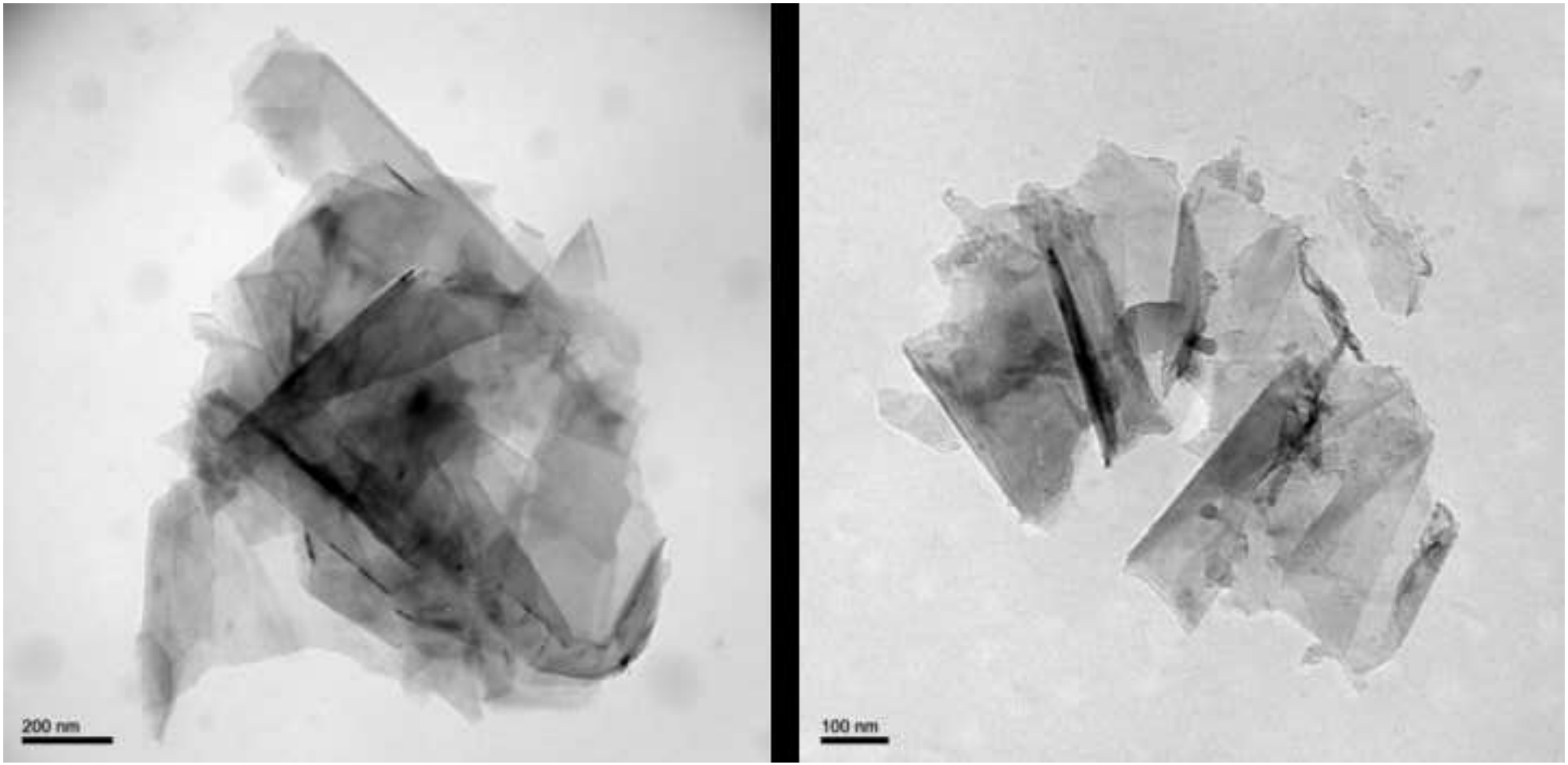

Figure 4

Click here to download high resolution image

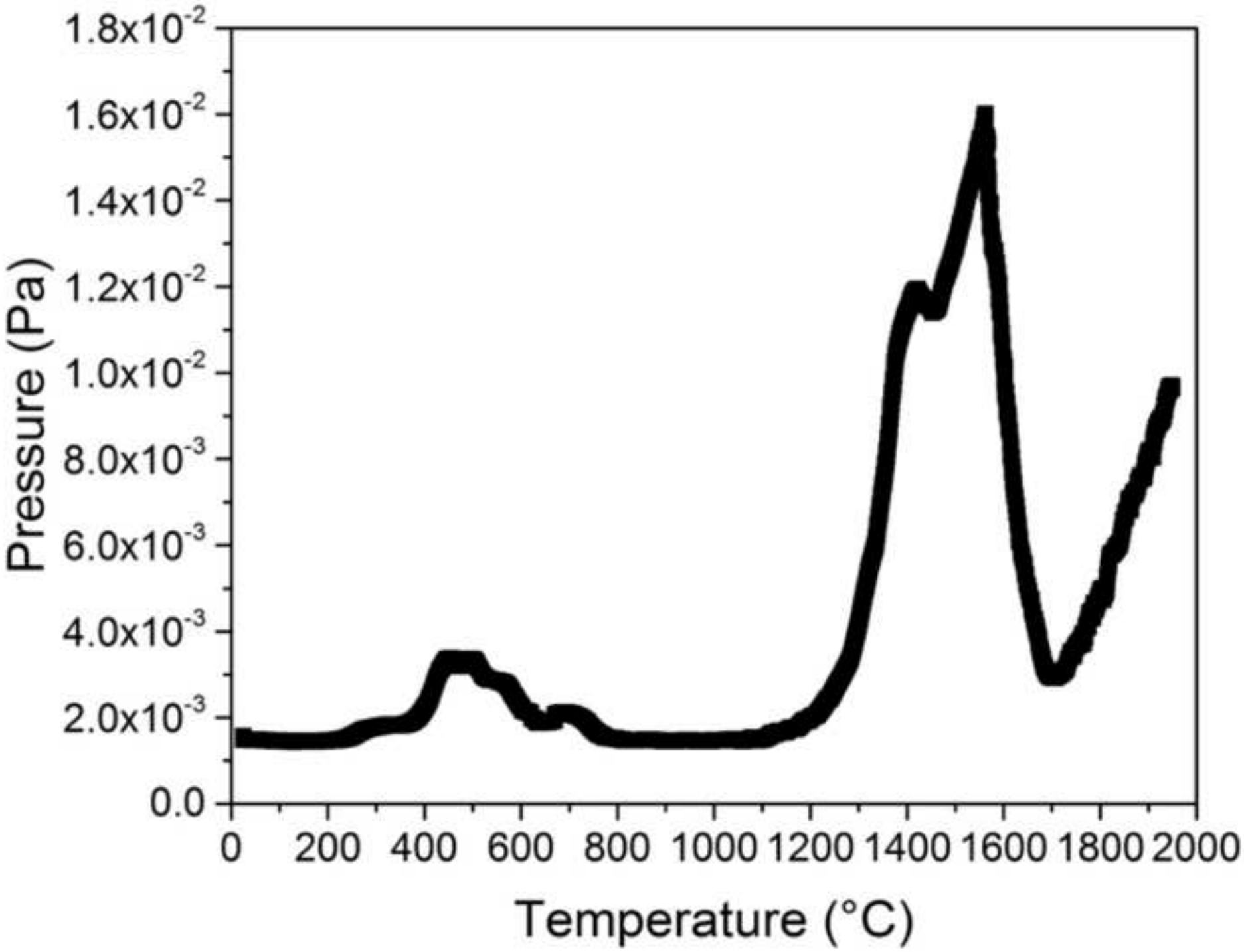

Figure 5

Click here to download high resolution image

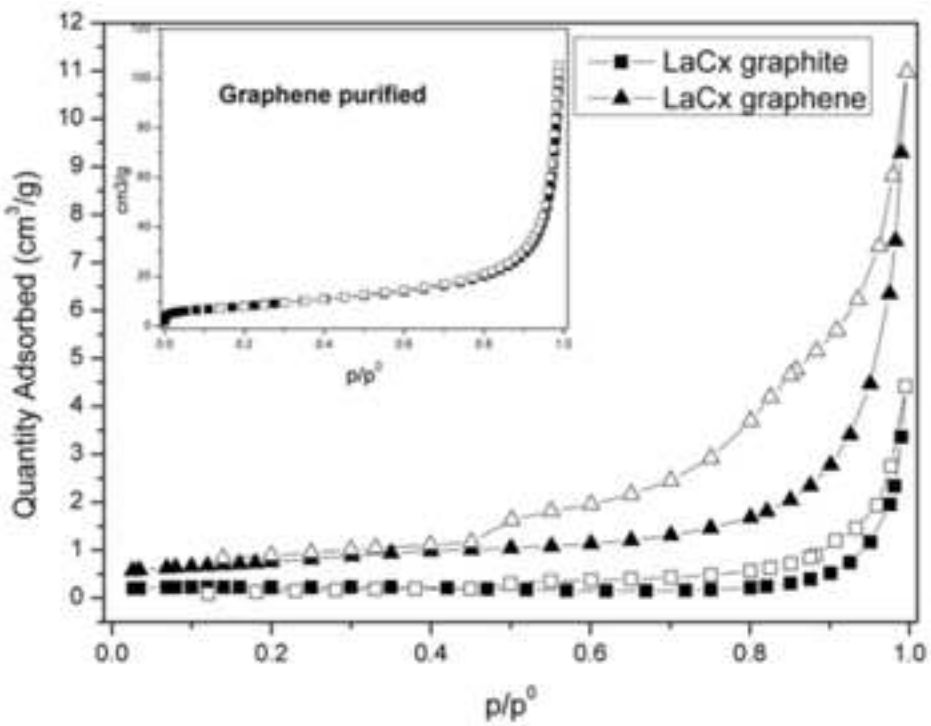

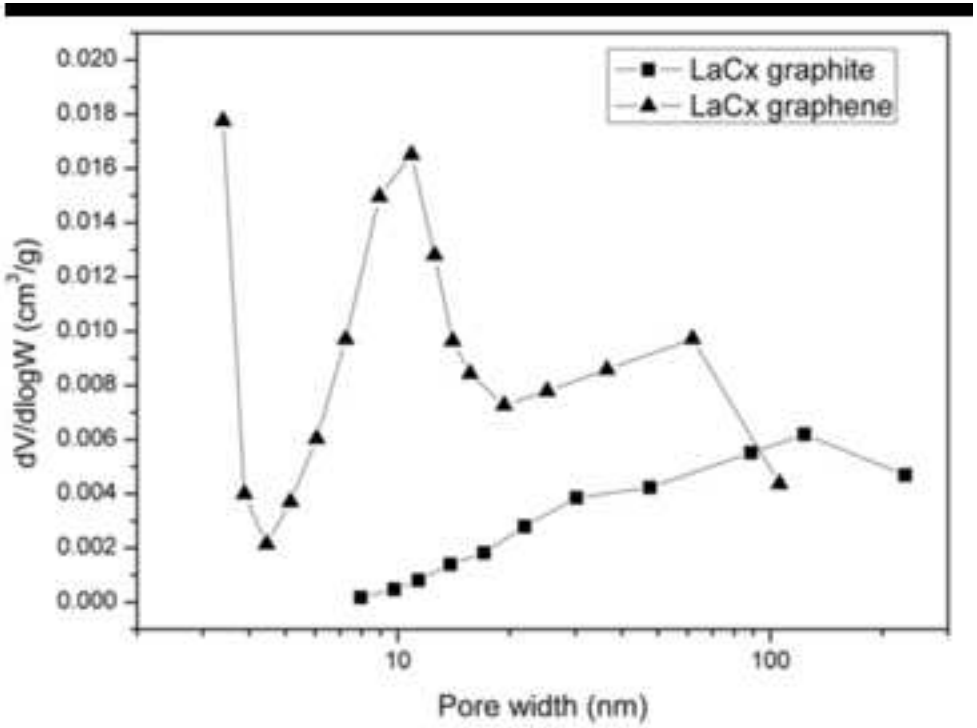

Figure 6

Click here to download high resolution image

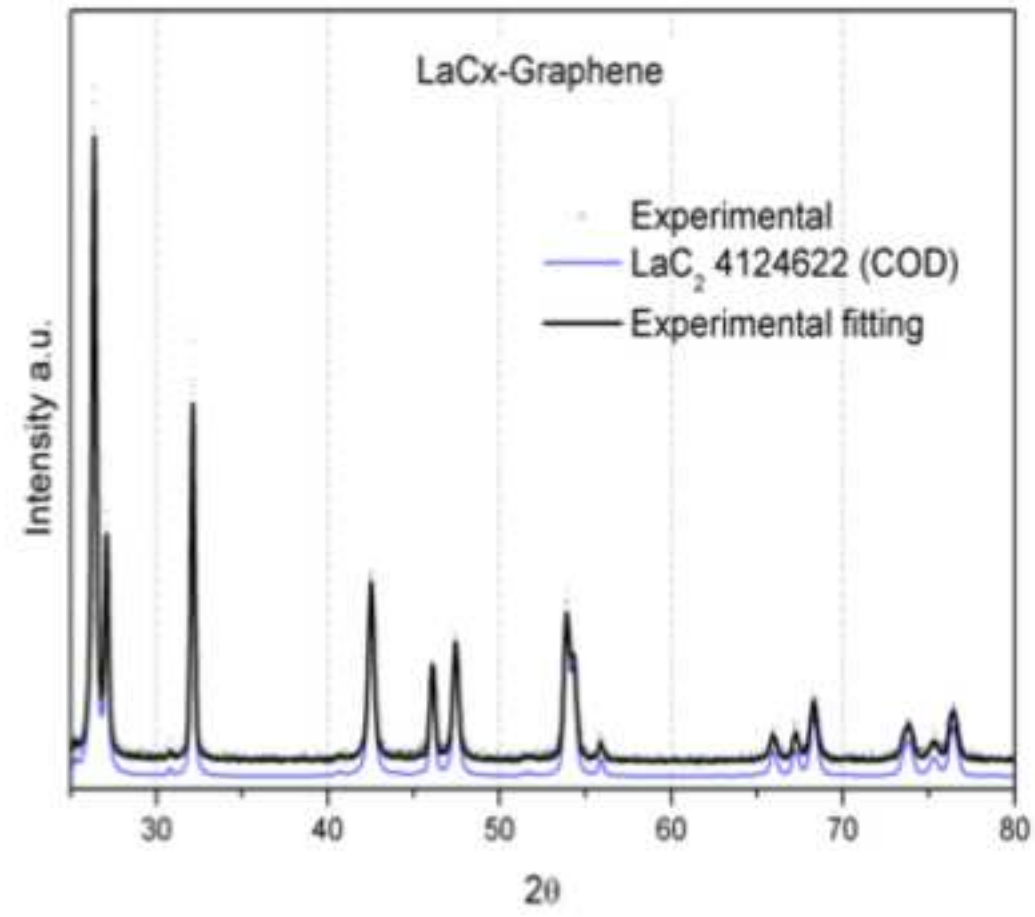

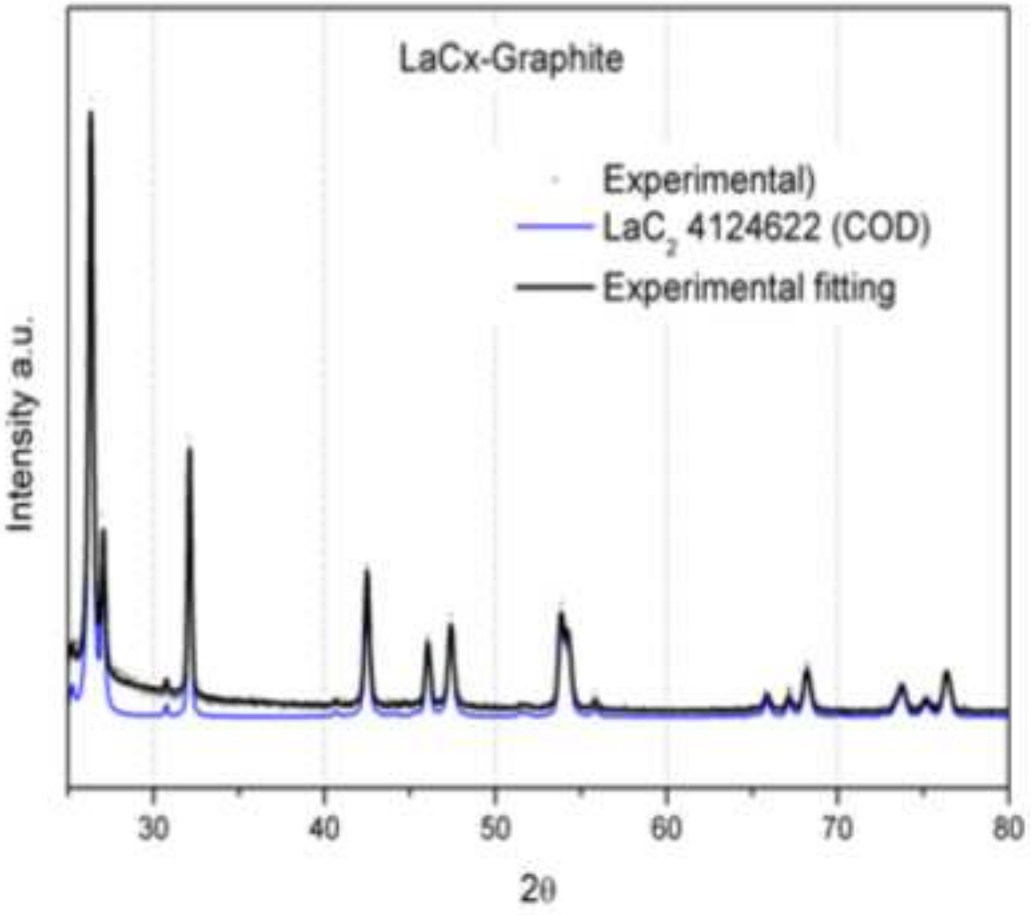

Figure 7

Click here to download high resolution image

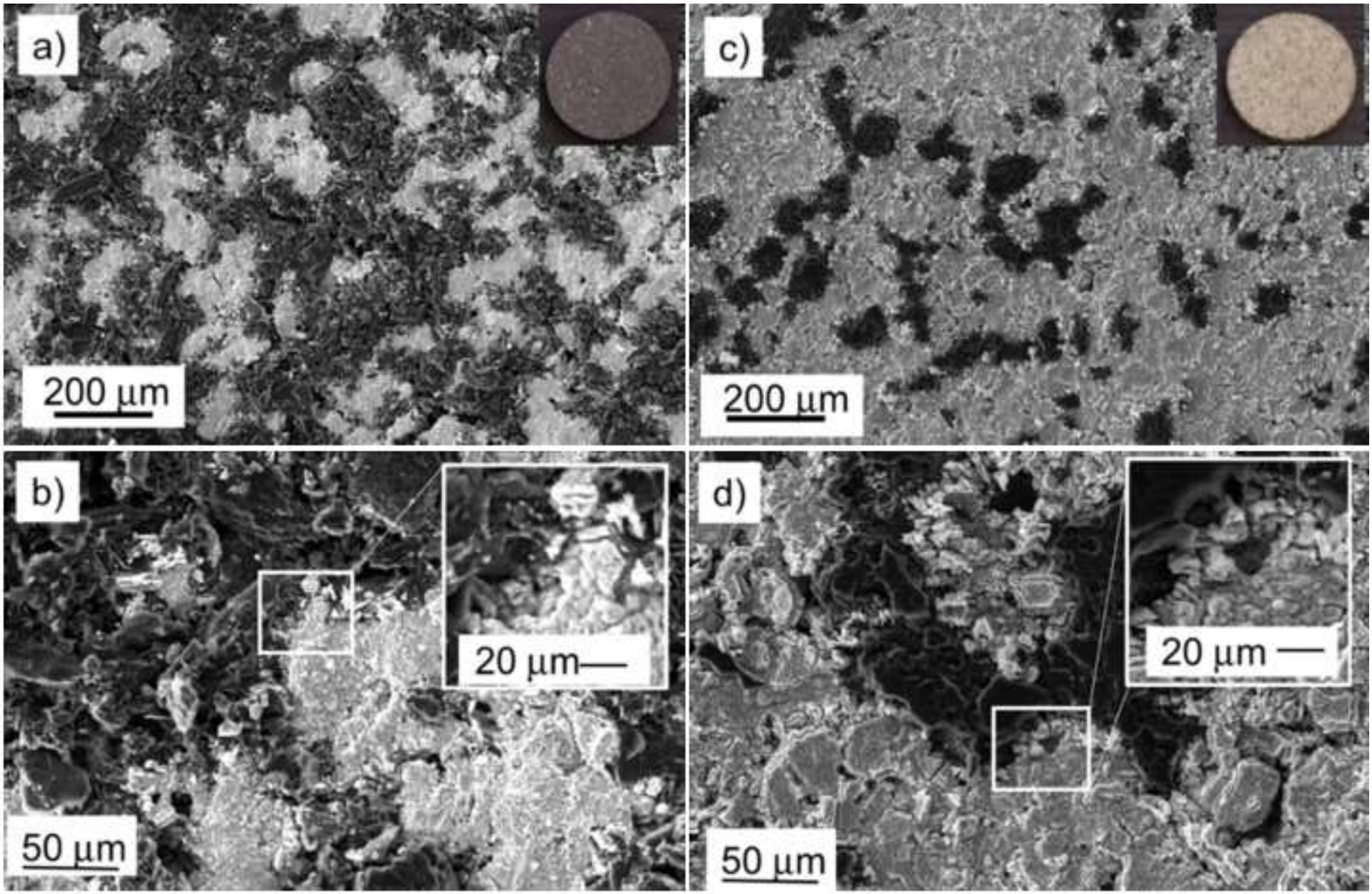

Figure 8

Click here to download high resolution image

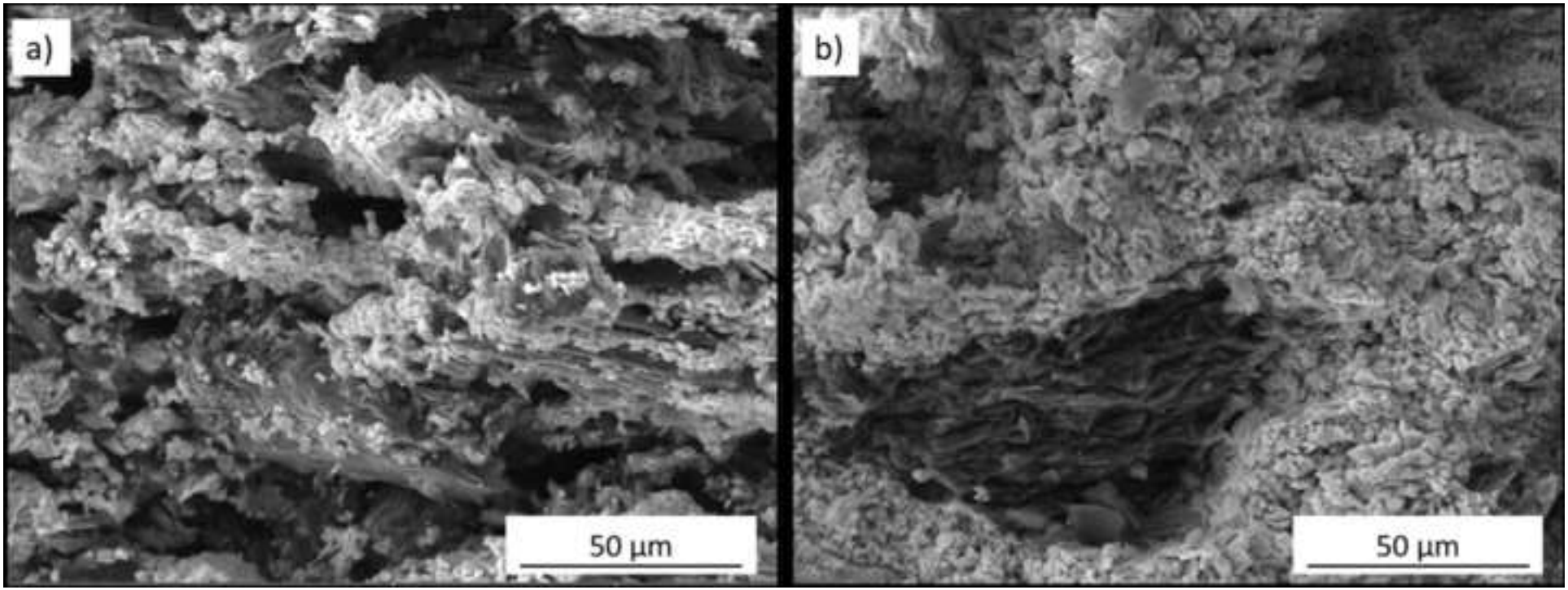

Figure 9

Click here to download high resolution image

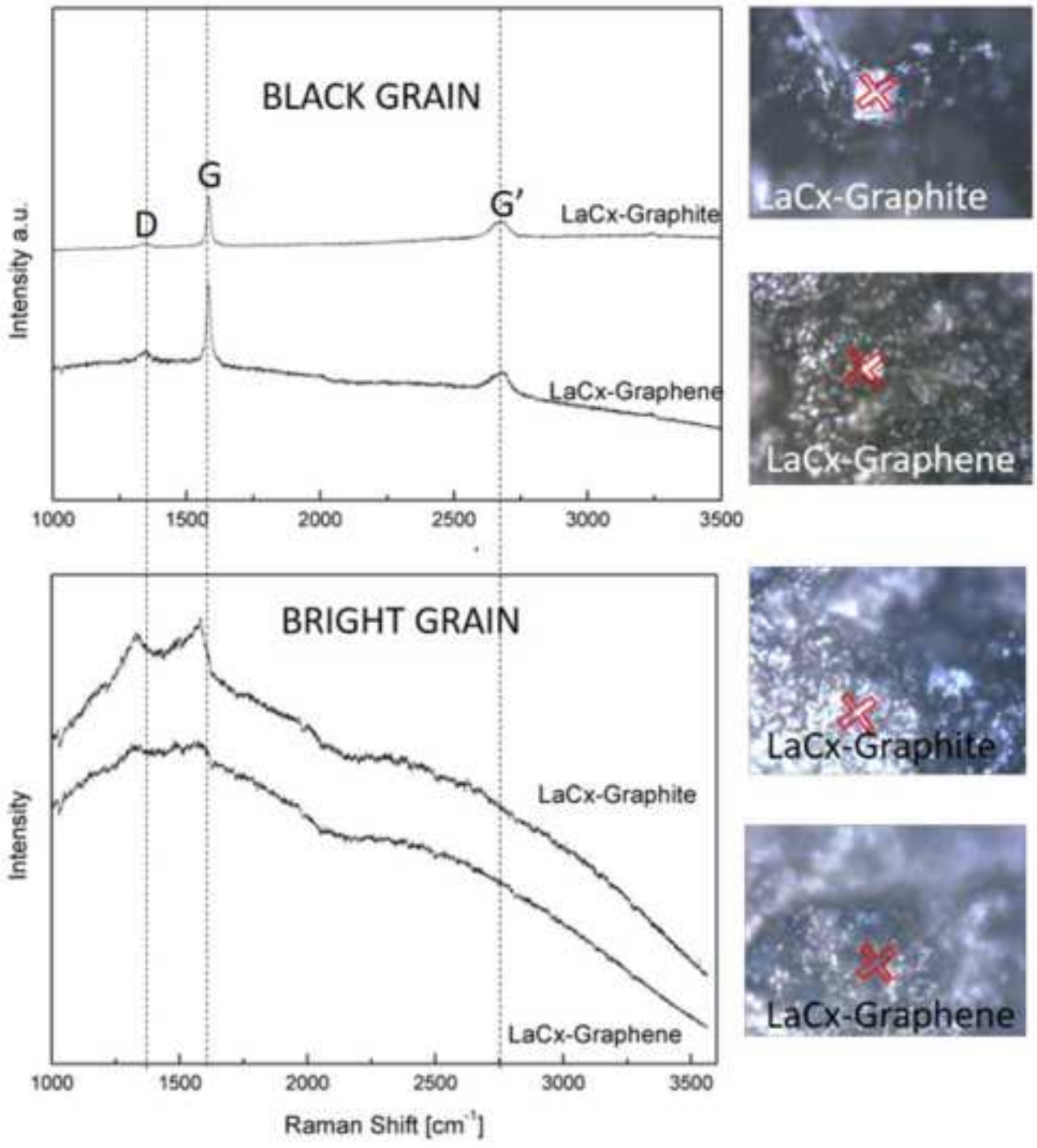

Table 1

Table 1

	I_D/I_G	L_a [nm]
Graphite	0.38	44.3
Graphene	1.08	15.6

Table 2

Table 2

Sample	Composition			Density [g/cm^3]	Shrinkage [vol.%]	Weight loss [wt.%]	Theoretical weight loss [wt.%]	Total porosity [vol.%]
	La_2O_3 [wt.%]	Graphite [wt.%]	Graphene [wt.%]					
LaCx-Graphite	71.2	28.8	-	3.1 ± 0.1	5.8 ± 0.6	23.8 ± 0.3	18.4	47.8 ± 1.0
LaCx-Graphene	71.2	-	28.8	2.2 ± 0.1	20.4 ± 3.1	22.2 ± 0.2	18.4	28.9 ± 2.2[a] 32.6 ± 2.1[b]

Tables and FiguresCaptions

Figure 1 – Graphite and Graphene Diffraction patterns

Figure 2- Left: Raman spectra of a.r. graphene and graphite; right: Lorentian peak fitting.

Table 2-Stacking layers calculation for a.r Graphene and Graphite

Figure 3- TEM micrographs of as received a) graphene and b) graphite powders.

Table 3- Composition, shrinkage, weight losses and calculated total porosity of the produced samples. [a] Data for $\rho\rho_{graphene}$ = 1.9 g/cm^3, [b] data for $\rho_{graphene}$ = 2.3 g/cm^3

Figure 4- Gas evolution upon carburization and sintering of graphene and graphite derived LaC_x (two samples for each composition treated together).

Figure 5- N_2 adsorption-desorption isotherms for LaCx composites derived from graphite or graphene (left side, inset graph graphene after purification) and pore size distribution as derived from BJH model (right side).

Figure 6- Top, XRD diffraction of LaC_x-Graphene; bottom XRD pattern of LaC_x-Graphite

Figure 7-SEM images of LaC_x-Graphite (a,b) and LaC_x-Graphene(c,d). The inserts in figures a and c show the samples after thermal treatment.

Figure 8. SEM images of the cross-section of the samples derived from graphite (a) and graphene (b) taken at the same magnification (1600x).

Figure 9- Raman spectra of LaC_x-Graphite and LaC_x-Graphene samples (black grain, unreacted carbon, while bright grain is the LaC_x grain.